Supplemental Information for

Theoretical Prediction of Graphene-like 2D Uranyl Material

with p-Orbital Antiferromagnetism

Xiao-Kun Zhao[1], Chang-Su Cao[1], Jin-Cheng Liu[1], Jun-Bo Lu[2], Jun Li[1,2] & Han-Shi Hu[1*]

[1]Department of Chemistry and Key Laboratory of Organic Optoelectronics & Molecular

Engineering of Ministry of Education, Tsinghua University, Beijing 100084, China

[2]Department of Chemistry, Southern University of Science and Technology, Shenzhen 518055,

China

E-mail: hshu@mail.tsinghua.edu.cn

Table of Contents

1. Theoretical and Computational Details

We applied USPEX program to perform fixed-composition global minimum (GM) searches based on the composition of $(UO_2)_2(\mu_2-O_2)_2(\mu_2-OH)_2$, the selection of which is to avoid formation of discrete small clusters in the presence of counterions. The first generation of 20 structures was generated using a random symmetric generator except the seed structure.[1, 2] The subsequent generations of 20 structures were generated with 50% heredity, 30% random symmetric and 20% soft mutation or coormutation generator. The USPEX GM searching progress was stopped when the best structure no longer changes for 10 generations with 197 structures in total. Moreover, the structure relaxations during the searching progress were performed using the density functional theory (DFT) with Perdew–Burke–Ernzerhof (PBE) functional, as implemented in VASP 5.4.4 program.[3, 4]

The most stable structures from the GM search were further refined via supercell calculations with VASP 5.4.4 program as well as cluster calculations with ADF 2019 and Gaussian 16 programs, respectively.[5, 6] In the supercell calculations, the plane-wave basis sets were adopted with 600 eV kinetic energy cutoff to approximate the valence electron densities. The projector augmented wave (PAW) method was used to account for the core–valence interaction.[7] The geometry optimization was performed with PBE exchange-correlation functional of generalized gradient approximation (GGA). The self-consistent field convergence criterion was set to 10^{-3} eV/Å and 10^{-6} eV, respectively. The Brillouin zone was sampled with a 4×4×1 gamma-centered Monkhorst–Pack k-points grid. The DFT-D3 semi-empirical van der Waals correction was included to deal with dispersion interactions.[8] The Heyd–Scuseria–Ernzerhof (HSE06)[9] hybrid functional was applied to calculate the band structures of optimized 2D uranyl monolayer sheet. We also evaluated the non-magnetic (NM), ferromagnetic (FM), and antiferromagnetic (AFM) states to determine the spin coupling formalism between the superoxido groups in the uranyl sheet. In order to evaluate the kinetic stability of the 2D uranyl sheet, phonon dispersion analysis was performed using the Phonopy code interfaced with the finite displacement method.[10]

To estimate the bonding interactions between the uranyl and superoxido/hydroxyl moieties, the calculations for the finite cluster model of $(UO_2)_6(\mu_2-O_2)_4(\mu_2-OH)_4^{4+}$ with a hexagonal ring obtained from the 2D uranyl sheet were performed with ADF 2019. The scalar relativistic effects were taken into account at the zero-order regular approximation (ZORA).[11] The Slater-type-orbital (STO) basis sets with the quality of triple-ζ plus polarization functions (TZP) were used and the frozen core approximations were applied to the $[1s^2]$ shell of O and $[1s^2–4f^{14}]$ shells of U.[12] The hybrid PBE0 functional with corresponding dispersion correction was applied to carry out the energy decomposition analysis with natural orbitals for chemical valence (EDA-NOCV).[13-16] The principal interacting orbital (PIO) analysis[17-19] was also performed with the uranyl dimer cluster models of $(UO_2)_2(\mu_2-O_2)(O_2)_2(OH)_4^{3-}$ and $(UO_2)_2(O_2)_4(\mu_2-OH)_2^{2-}$ by using the PBE0 functional with 6-31+G* basis sets for H and O. The Stuttgart small-core energy-consistent relativistic

pseudopotential (ECP60MWB) with the corresponding ECP60MWB_SEG basis set were used for U in the Gaussian 16 calculations.[20, 21]

To explore the thermal stability, the *ab initio* molecular dynamics (AIMD) simulations were carried out by applying the Quickstep module with the PBE functional implemented in the CP2K simulation package at various temperatures within the range of 100–1000 K.[22] In the AIMD simulations, the wavefunction was expanded by mixed Gaussian and plane-wave basis sets with an energy cutoff of 500 Ry for the plane wave,[23, 24] and molecularly optimized double-ζ valence plus polarization basis sets were used to minimize the basis set superposition errors. The recently developed Geodecker–Teter–Hutter (GTH) pseudopotentials by Lu et al. were also adopted to model the core electrons with 14 valence electrons for U, 6 valence electrons for O, and 1 valence electron for H, respectively.[25] Reciprocal space mesh consisting of gamma point was used for Brillouin zone integration. In addition, the initial configurations of the 2D uranyl sheet with 4×4×1 supercell (32 U atoms, 160 O atoms and 32 H atoms) was annealed at different temperatures. MD simulations in canonical (NVT) ensemble last 10 ps for 300, 400, 500, 600 K and 5 ps for 1000 K with a time step of 0.5 fs, and the temperature was controlled by employing Nose–Hoover thermostats.[26, 27]
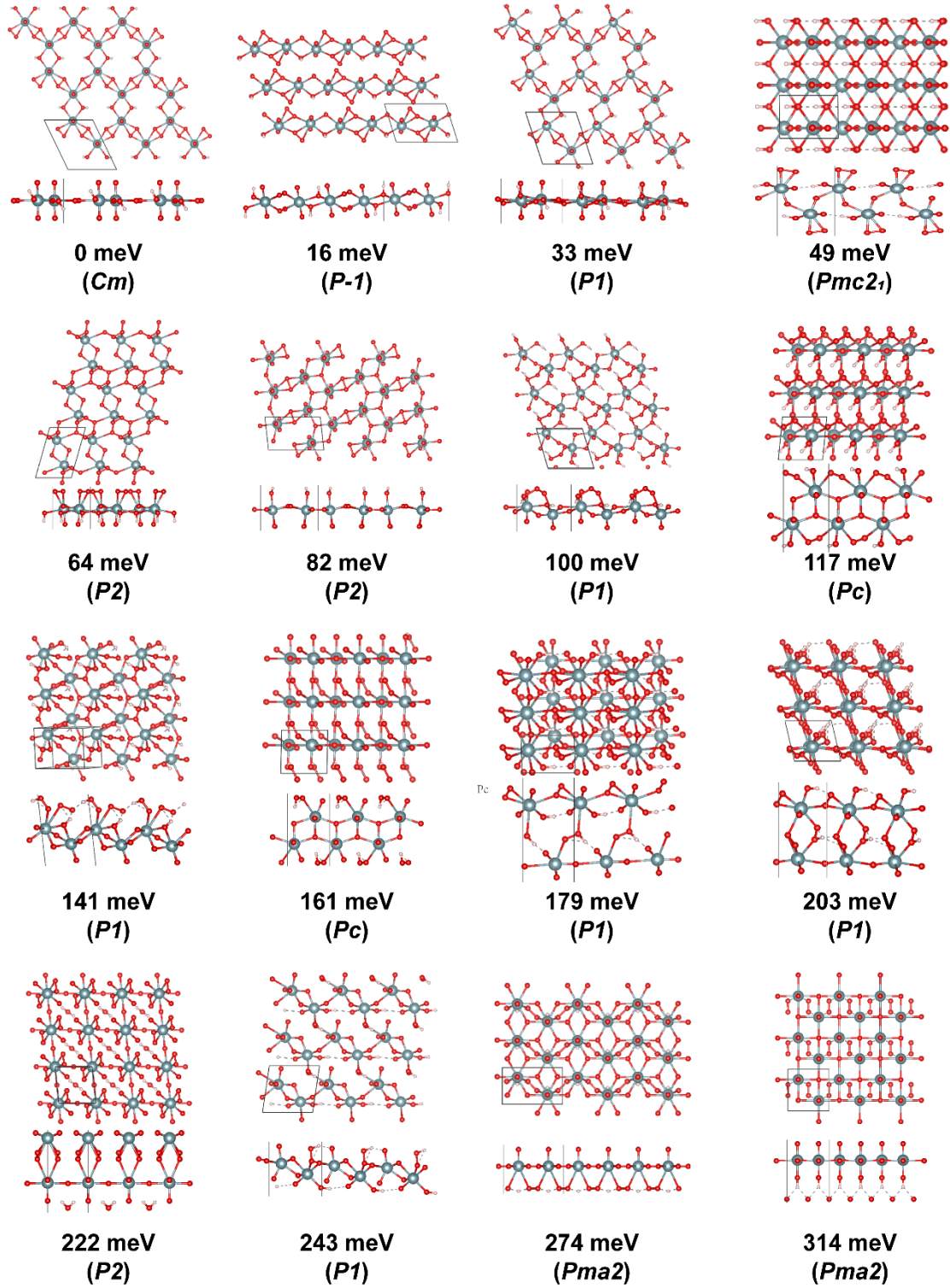
2. Supplementary Figures

Figure S1. Top view (upper) and side view (lower) of the low-energy 2D structures of 2D uranyl sheet obtained from the USPEX simulations. The relative energy per atom and corresponding space groups (in parentheses) are indicated. Uranium, oxygen and hydrogen atoms are in gray, red and white colors, respectively.
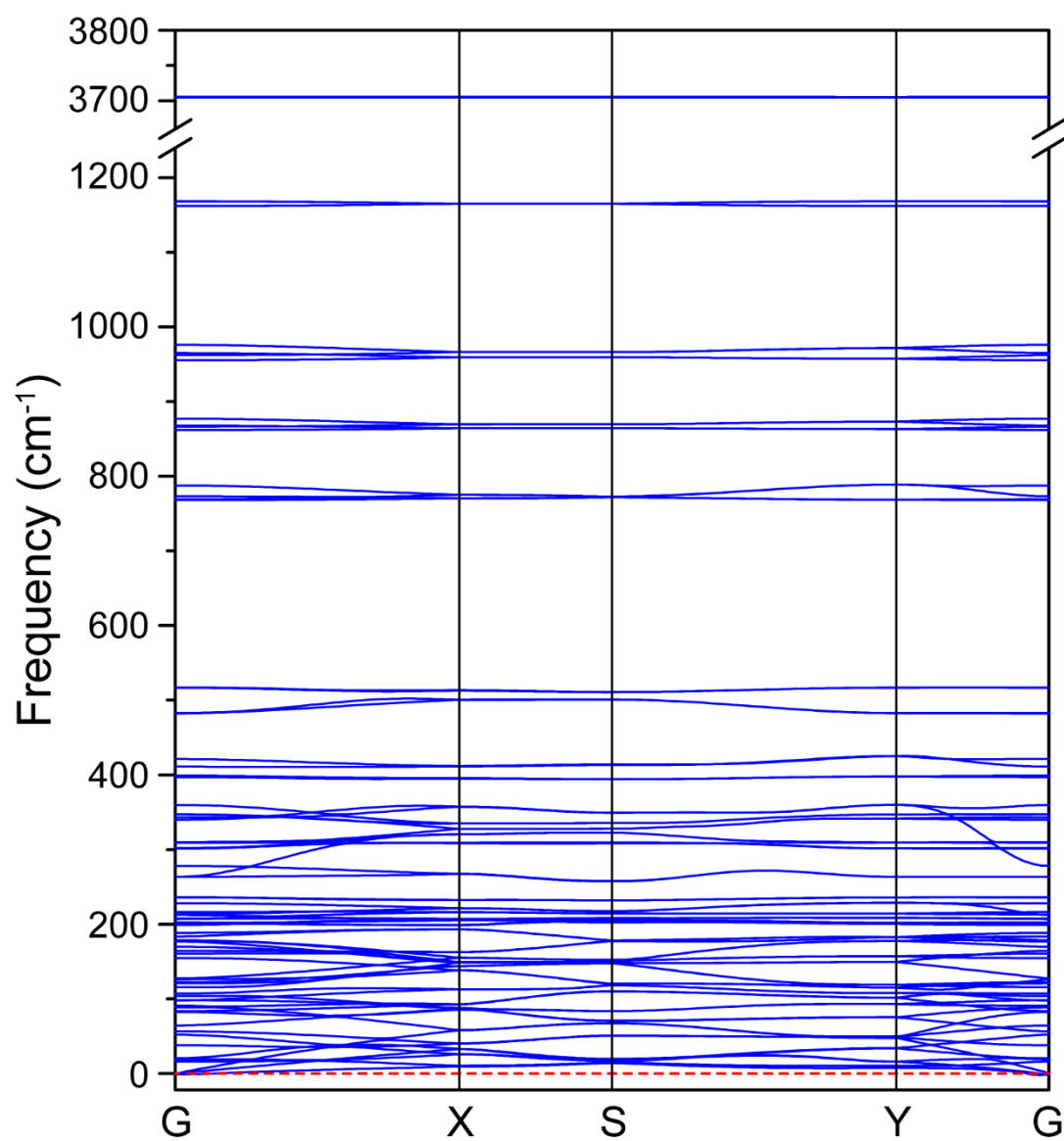
Figure S2. Phonon spectrum of optimized 2D uranyl sheet. The red dashed line is set to zero. G (0, 0, 0), X (0.5, 0, 0), S (0.5, 0.5, 0) and Y (0, 0.5, 0) refer to high-symmetry points in the first Brillouin zone in reciprocal space.
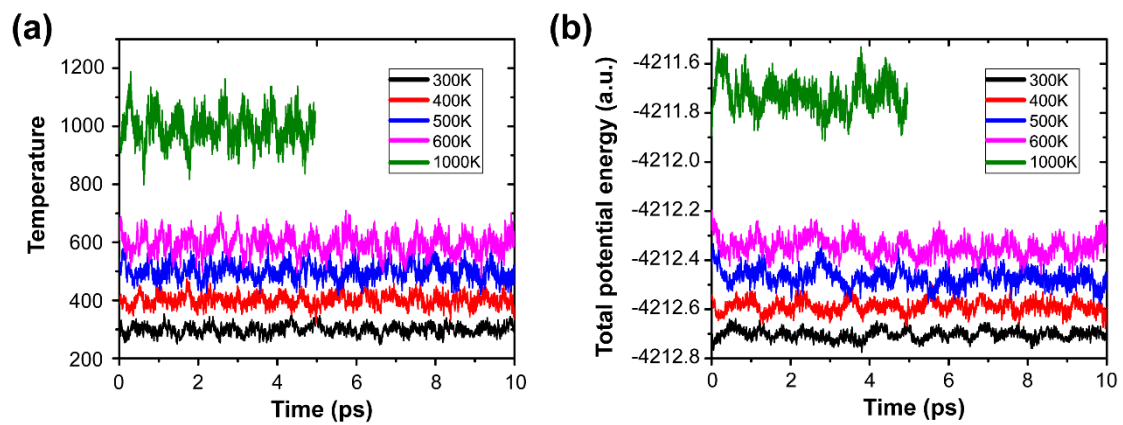
Figure S3. Fluctuations of **(a)** temperature and **(b)** total potential energy for the uranyl monolayer at different temperatures during the AIMD simulations with spin-polarization.
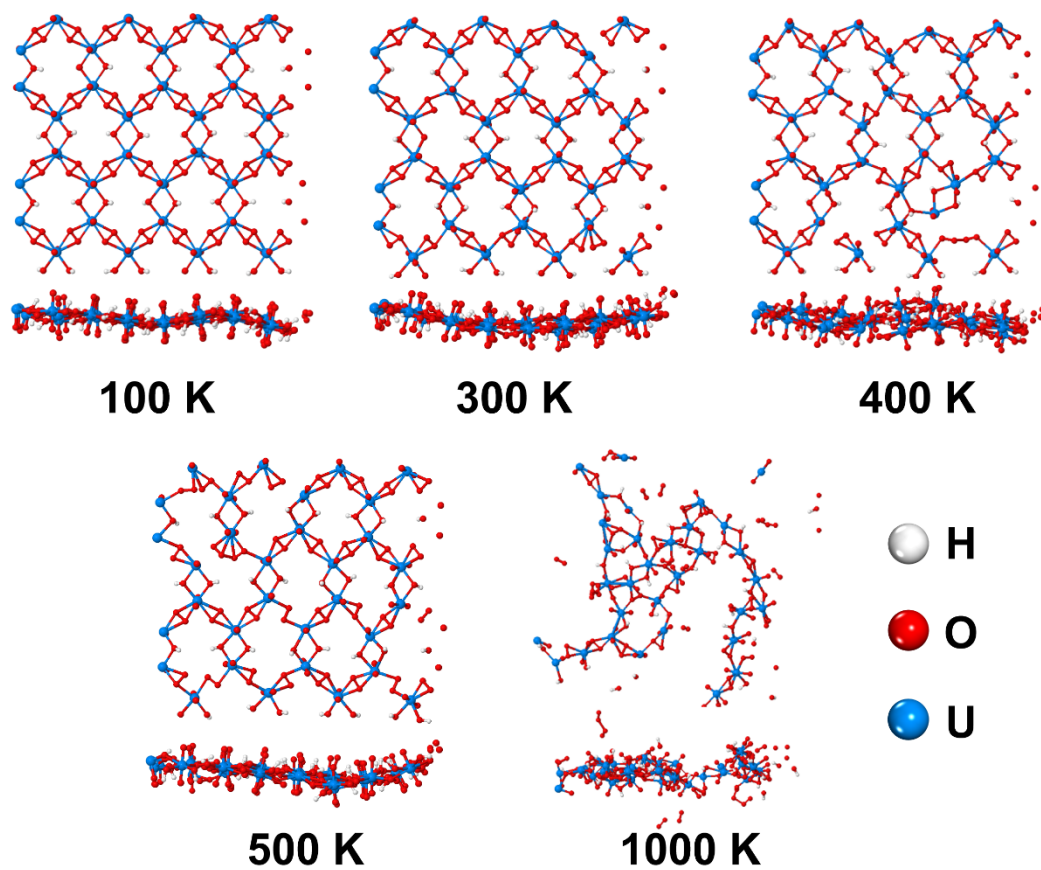
Figure S4. Snapshots of the final frame of each AIMD simulation without spin polarization from 100 to 1000 K (top and side views). Bonds to atoms outside this 4 × 4 section exist but are not shown.
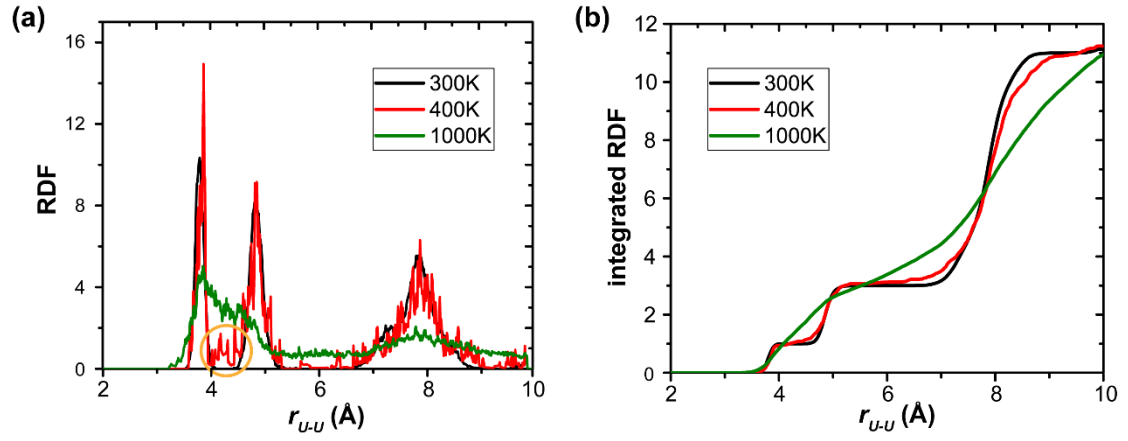
Figure S5. The radial distribution function (RDF) of U-U distance at different temperatures: RDF (a) and integrated RDF (b) for non-spin-polarized calculations.
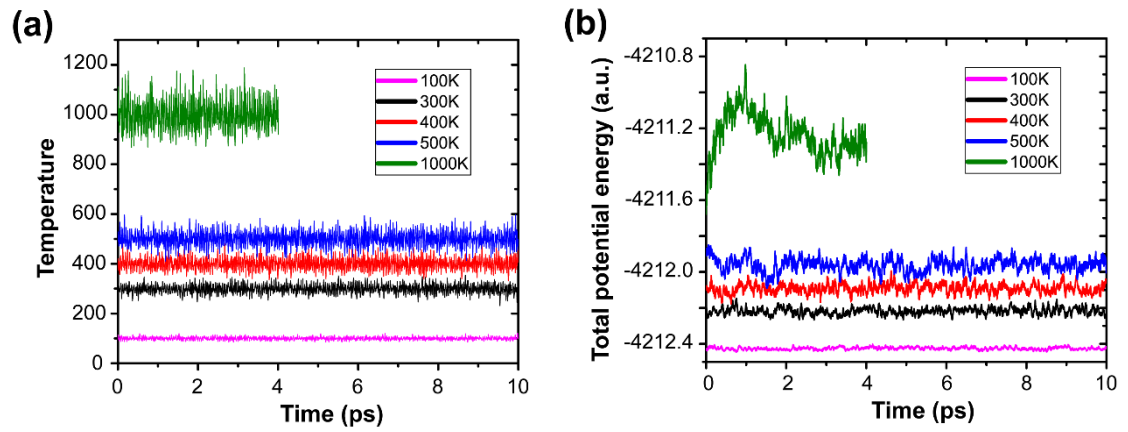

Figure S6. Fluctuations of **(a)** temperature and **(b)** total potential energy for the uranyl monolayer at different temperatures during AIMD simulations without spin polarization.
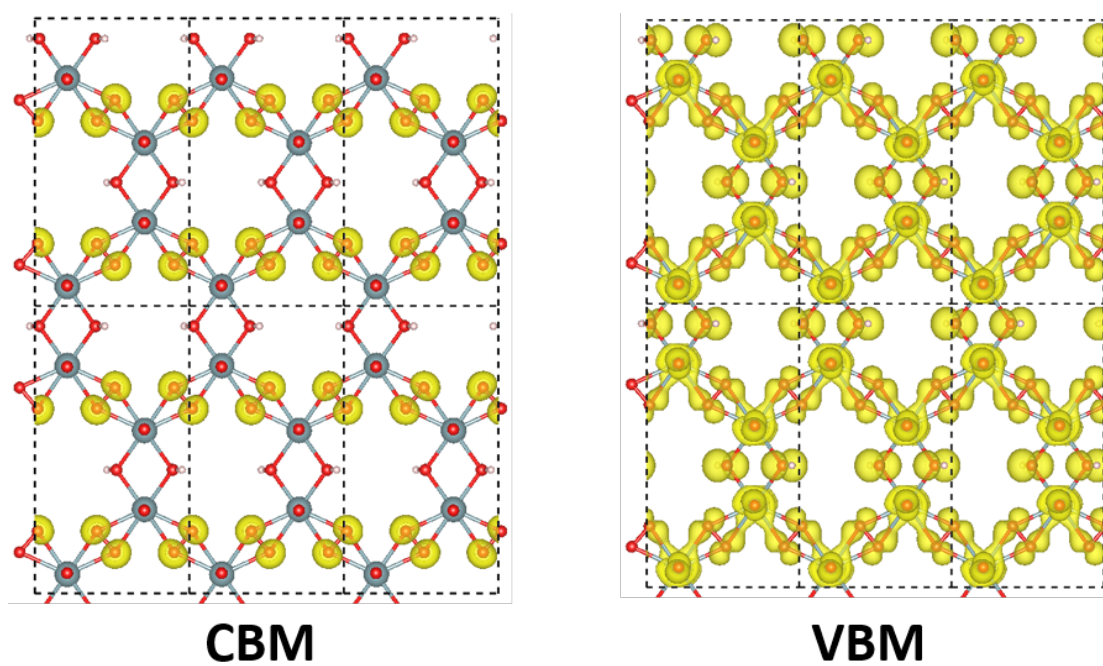
CBM

VBM

Figure S7. The partial charge densities for the conduction band minimum (CBM) and valence band maximum (VBM) at the gamma point.
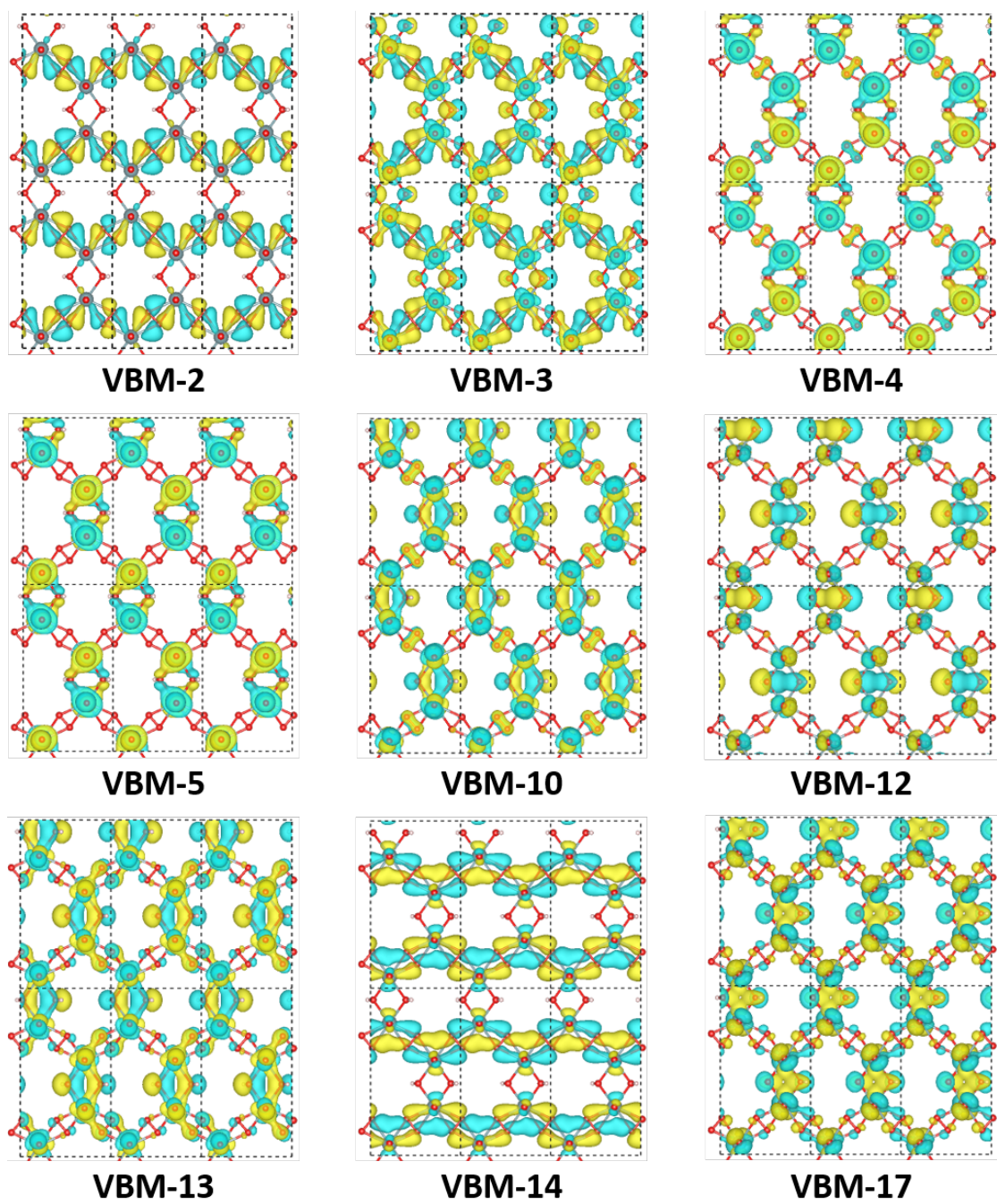
Figure S8. The real space wavefunctions for bands at the gamma point of 2D uranyl sheet.
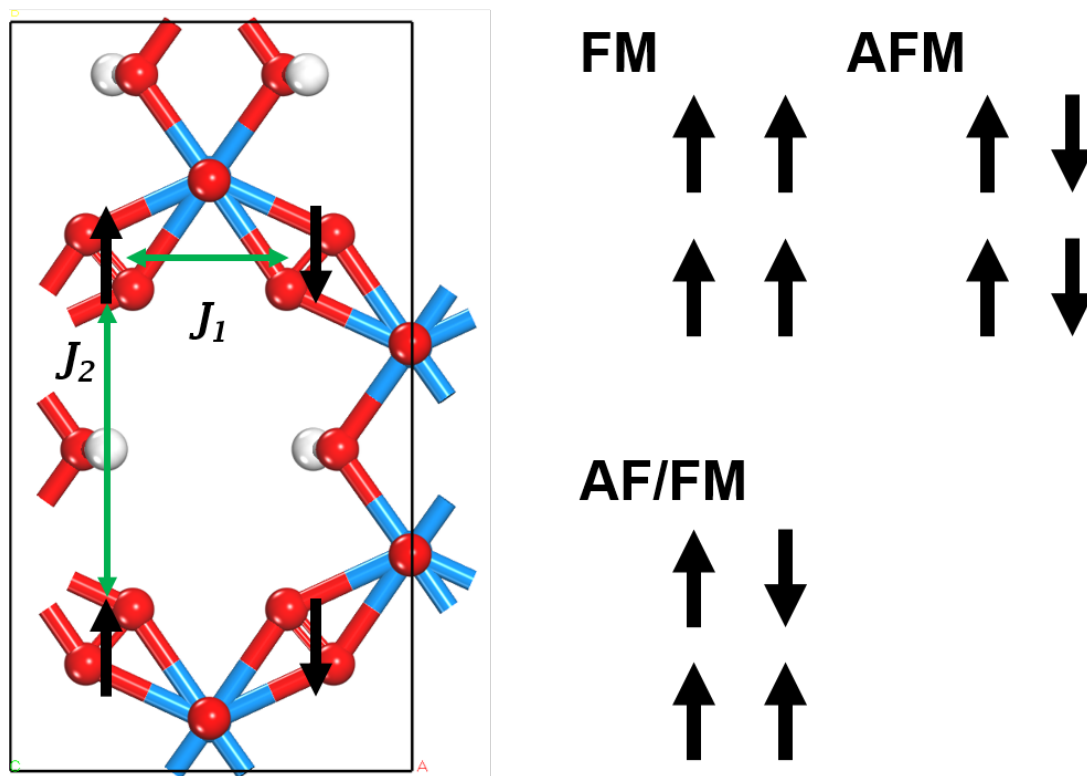
Figure S9. The schematic Heisenberg model of 2D uranyl sheet (left) and corresponding different magnetic states (right), where FM, AFM and AF/FM refer to three different magnetic states of ferromagnetic (FM), antiferromagnetic (AFM) and antiferromagnetic/ferromagnetic (AF/FM), respectively.
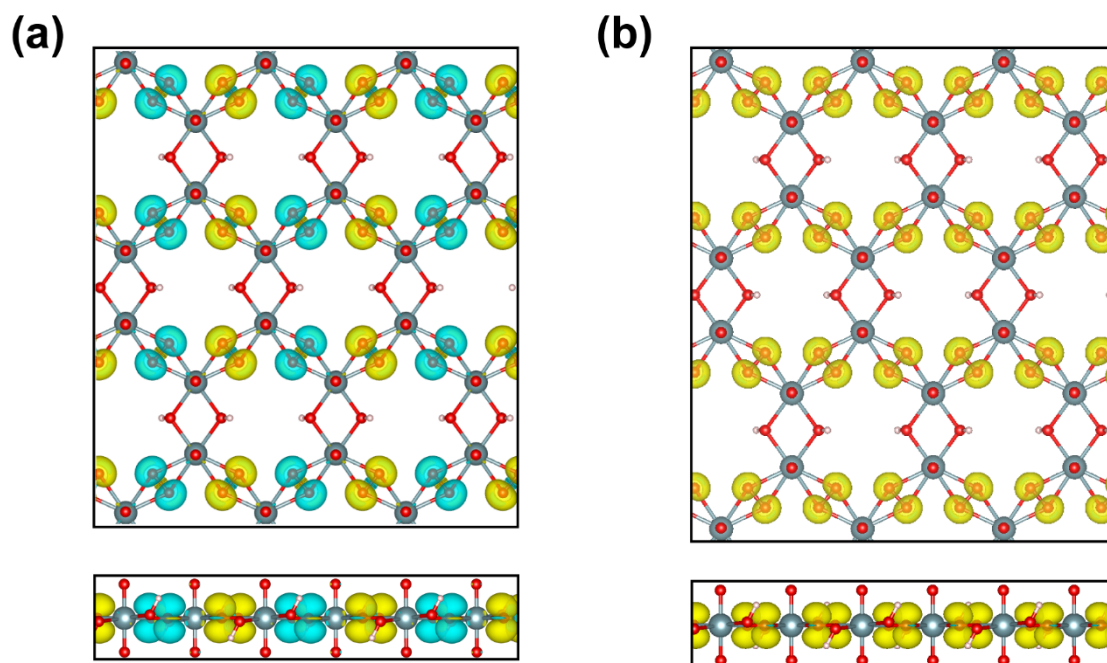
Figure S10. (a) Top (upper) and side (lower) view of spin density of 2D uranyl monolayer for AFM situation. **(b)** Top (upper) and side (lower) view of spin density of 2D uranyl monolayer for FM situation. The yellow isosurface is for spin up and blue for spin down. The isovalue is 0.005 e A^{-3}.

(a)

36.4 %
PIMO 1

18.3 %
PIMO 2

14.3 %
PIMO 3

13.3 %
PIMO 4

12.0 %
PIMO 5

(b)

21.2 %
PIMO 1

20.7 %
PIMO 2

16.2 %
PIMO 3
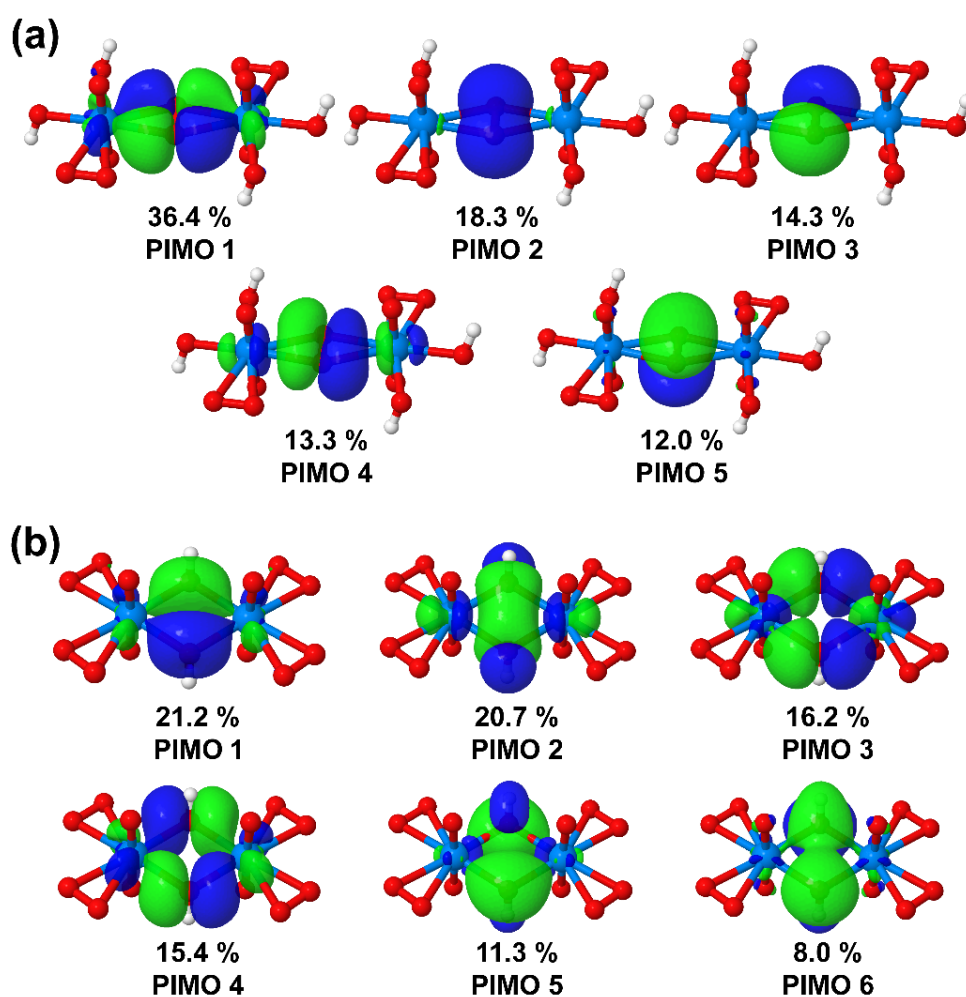
15.4 %
PIMO 4

11.3 %
PIMO 5

8.0 %
PIMO 6

Figure S11. Results of principal interacting orbital (PIO) analysis. **(a)** The top five PIMO pairs between the superoxide (O_2^-) fragment and uranyl fragments. **(b)** The top six PIMO pairs between the hydroxyl (OH^-) fragments and uranyl fragments. (isovalue = 0.02)
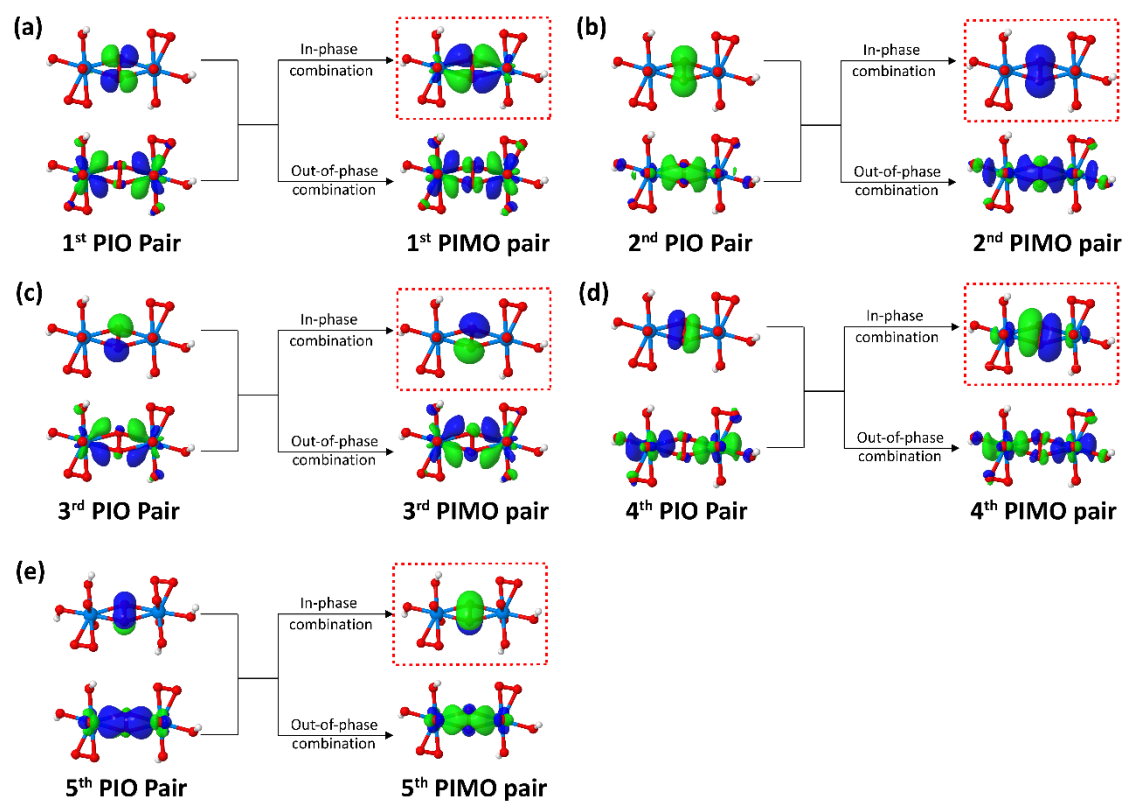
Figure S12. The top five principal interacting molecular orbital (PIMO) pairs and their relationship with the corresponding PIO pair. Note that the phase of each PIO is naturally paired up with its counterpart. (isosurface = 0.03)
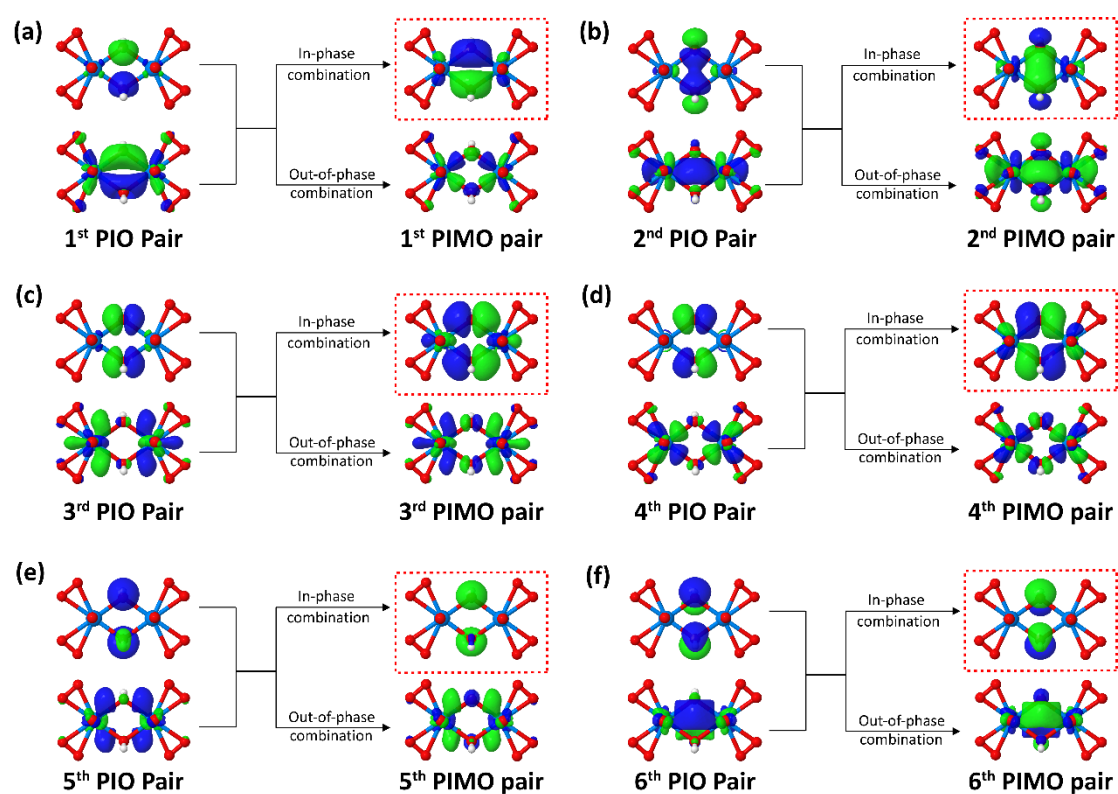
Figure S13. The top six principal interacting molecular orbital (PIMO) pairs and their relationship with the corresponding PIO pair. Note that the phase of each PIO is naturally paired up with its counterpart. (isosurface = 0.03)
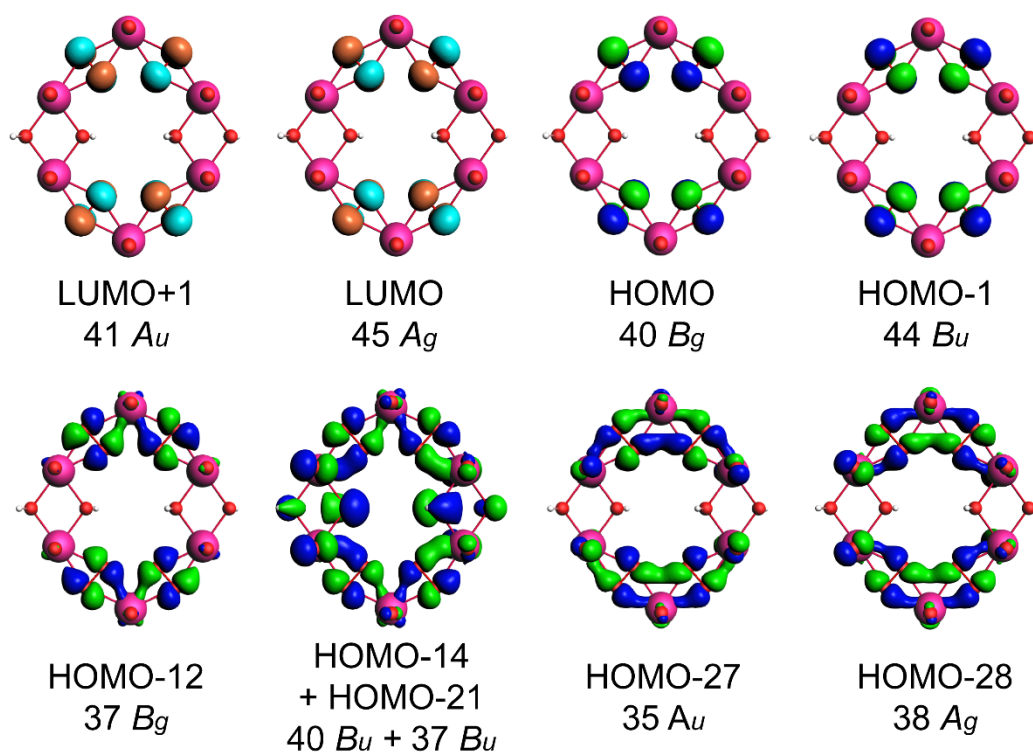
Figure S14. Kohn-Sham $2p_{\pi^*}$ orbitals of superoxido groups in the hexagonal uranyl-unit ring ($[(UO_2)_6(\mu_2\text{-}O_2)_4(\mu_2\text{-}OH)_4]^{4+}$). (isosurface = 0.03)

3. Supplementary Tables

Table S1. The calculated single point energy of the most stable four isomers by employing DFT functionals of PBE and HSE06 based on the geometry structures from USPEX global minimum search (the energy is in meV per atom.)
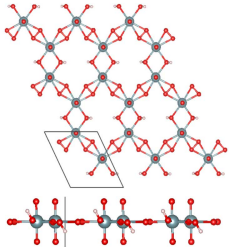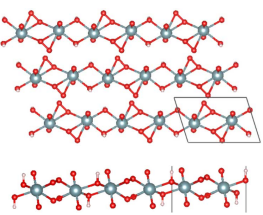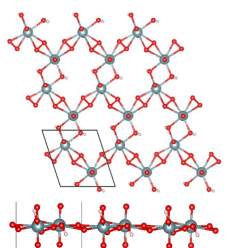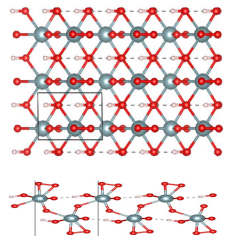
Isomers	PBE level	HSE 06 level
(Cm)	0	0
(P-1)	16	106
(P1)	33	151
(Pmc2$_1$)	49	269

Table S2. Comparison of experimental [U_{60}] cluster and computationally optimized 2D uranyl sheet geometries.

	Exp. Data[28]				Comput. Data
	O_2	O_2^-	O_2^{2-}	[U_{60}] cluster	2D uranyl sheet
[a]$R_{(O-O)}$ /Å	1.21	1.33	1.49	1.46 – 1.69[a]	1.34[a]
$R_{(HO-OH)}$ /Å		-		2.71 – 2.77	2.76
$R_{(O-H)}$ /Å		-		-	0.98
[b]$R_{(U-O)}$ /Å		-		1.76 – 1.84	1.80
$\angle$(O-U-O)				178.7 – 179.5°	177.9°
$\angle$(U-O_2-U)		-		143.2 – 159.7°	180.0°
$\angle$(U-$(OH)_2$-U)		-		174.0 – 175.0°	180.0°

[a]The O-O bond length of O_2 moieties in [U_{60}] cluster and 2D uranyl sheet.

[b]The U-O bond length of uranyl in [U_{60}] cluster and 2D uranyl sheet.

Table S3. The formation energy of 2D uranyl sheet from water, oxygen and uranium dioxide solid at ambient temperature and pressure (300 K, 1 atm).

	E /eV	Correction /eV	Gibbs free energy /eV
H_2O	-14.236	-0.007	-14.242
O_2	-9.865	-0.447	-10.313
UO_2	-31.542	0.058	-31.484
$U_4H_4O_{20}$	-209.200	1.426	-207.774

2 H_2O + 5 O_2 + 4 UO_2 → $(UO_2)_4(\mu_2\text{-}O_2)_4(\mu_2\text{-}OH)_4$ ΔG_{300K} = -1.789 eV = -41.3 kcal/mol
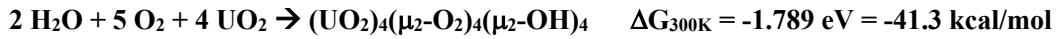
Table S4. The electronic energy (eV) of the 2D uranyl sheet for non-magnetic (NM), ferromagnetic (FM), and antiferromagnetic (AFM) states, respectively. The calculation model includes 4 U atoms, 20 O atoms and 4 H atoms in a unit cell.
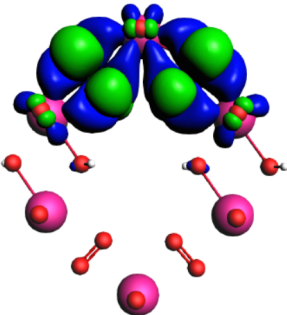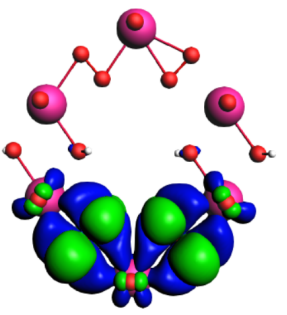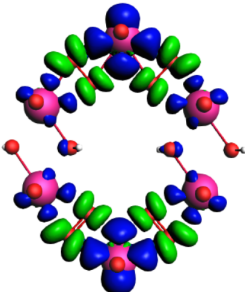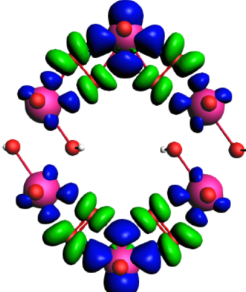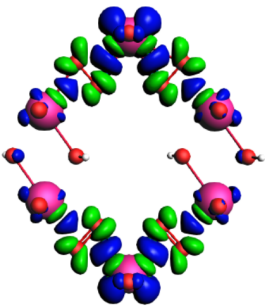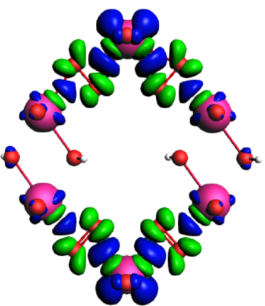
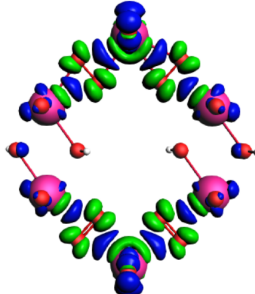|	Energy (eV)
NM	-207.829
FM	-209.081
AFM	-209.200
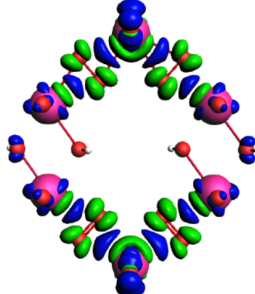
Table S5. The calculated energies with seven types of different spin orientations for the 2D uranyl sheet with the unit cell containing four superoxido groups.

Spin direction plane	Energy (eV)
(0 0 1)	-218.1985992
(0 1 0)	-218.1983624
(1 0 0)	-218.1983968
(0 1 1)	-218.1984808
(1 0 1)	-218.1985469
(1 1 0)	-218.1983796
(1 1 1)	-218.1984854

As we can see from the results in table S5 above, the most stable one is with the spins orientating along the (0 0 1) plane and the most unstable one with the spins orientating along the (0 1 0) plane. Therefore, the magnetic anisotropy energy (MAE) value is obtained by $E_{MAE} = E_{(0\,0\,1)} - E_{(0\,1\,0)} = 0.06$ meV/superoxido group.

Table S6. Energy decomposition analysis (EDA) of the $(UO_2)_6(\mu_2\text{-}O_2)_4(\mu_2\text{-}OH)_4^{4+}$ at the PBE0/TZP level and the associated deformation densities $\Delta\rho$ of the most important pairwise orbital interactions ΔE_{orb} (isosurfaces = 0.0003 au). The direction of the charge flow is green to blue. Energy values are given in kcal·mol^{-1}.
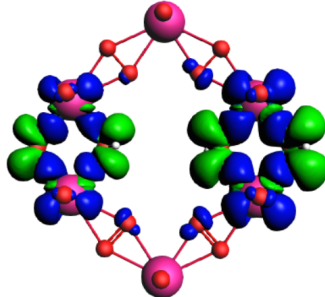
	fragment 1: $(\mu_2\text{-}O_2)_4^{4-}$ fragment 2: $(UO_2)_6(\mu_2\text{-}OH)_4^{8+}$	
ΔE_{int}	-2715.71	
ΔE_{Pauli}	459.12	
ΔE_{elstat}[a]	-2734.64 (86.1%)	
ΔE_{orb}[a]	-434.59 (13.7%)	
ΔE_{disp}[a]	-5.61 (0.2%)	
$\Delta E_{orb(\pi_1)}$[b]		
	-74.67 17.2%	-74.79 17.2%
$\Delta E_{orb(\pi_2)}$[b]		
	-34.34 7.9%	-34.55 7.9%
$\Delta E_{orb(\sigma_1)}$[b]		
	-19.37 4.5%	-19.27 4.4%
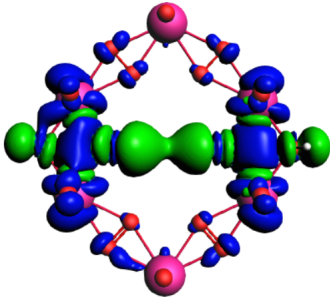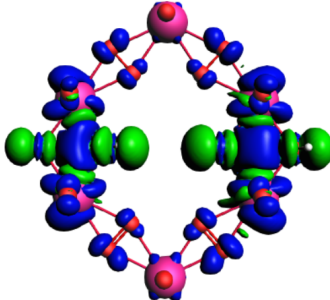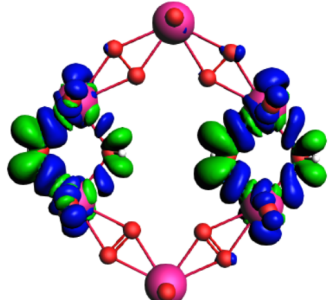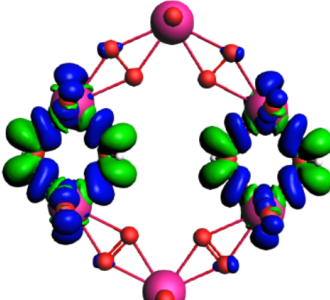
$\Delta E_{\mathrm{orb}(\sigma_2)}$[b]		
	-14.58 3.4%	-14.54 3.3%

[a] The value in parentheses gives the percentage contribution to the total attractive interaction, $\Delta E_{\mathrm{elstat}}$ + ΔE_{orb} + ΔE_{disp}.

[b] The values in parentheses give the percentage contribution to the total orbital interaction, ΔE_{orb}.

Table S7. Energy decomposition analysis (EDA) of the $(UO_2)_6(\mu_2\text{-}O_2)_4(\mu_2\text{-}OH)_4^{4+}$ at the PBE0/TZP level and the associated deformation densities $\Delta\rho$ of the most important pairwise orbital interactions ΔE_{orb} (isosurfaces = 0.0003 au). The direction of the charge flow is green to blue. Energy values are given in kcal·mol^{-1}.
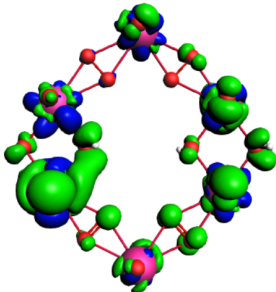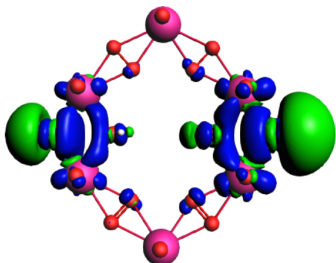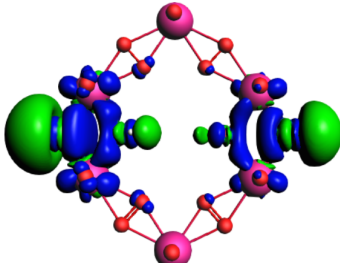
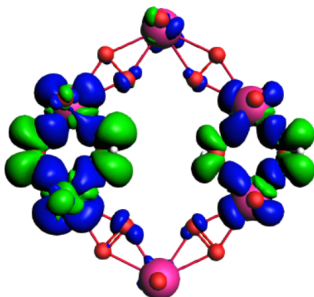|	fragment 1: $(\mu_2\text{-}OH)_4^{4-}$ fragment 2: $(UO_2)_6(\mu_2\text{-}O_2)_4^{8+}$	
ΔE_{int}	-249.93	
ΔE_{Pauli}	317.80	
$\Delta E_{elstat}{}^{a}$	-268.13 (47.2%)	
$\Delta E_{orb}{}^{a}$	-296.06 (52.1%)	
$\Delta E_{disp}{}^{a}$	-3.55 (0.6%)	
$\Delta E_{orb(1)}{}^{b}$		
	-82.27 9.9%	
$\Delta E_{orb(\pi_1)}{}^{b}$		
	-66.78 8.0%	-65.50 7.9%
$\Delta E_{orb(\pi_2)}{}^{b}$		
	-71.65 8.6%	-48.62 5.8%

$\Delta E_{orb(\sigma_1)}{}^{b}$		
	-44.30 5.3%	-44.21 5.3%
$\Delta E_{orb(\sigma_2)}{}^{b}$		
	-28.95 3.5%	-25.84 3.1%

[a] The value in parentheses gives the percentage contribution to the total attractive interaction, ΔE_{elstat} + ΔE_{orb} + ΔE_{disp}.

[b] The values in parentheses give the percentage contribution to the total orbital interaction, ΔE_{orb}.

4. References

1. Glass, C. W.; Oganov, A. R.; Hansen, N., USPEX–Evolutionary crystal structure prediction. *Comput. Phys. Commun.* **2006,** *175*, 713-720.

2. Lyakhov, A. O.; Oganov, A. R.; Stokes, H. T.; Zhu, Q., New developments in evolutionary structure prediction algorithm USPEX. *Comput. Phys. Commun.* **2013,** *184*, 1172-1182.

3. Kresse, G.; Furthmüller, J., Efficiency of ab-initio total energy calculations for metals and semiconductors using a plane-wave basis set. *Comput. Mater. Sci.* **1996,** *6*, 15-50.

4. Perdew, J. P.; Burke, K.; Ernzerhof, M., Generalized Gradient Approximation Made Simple. *Phys. Rev. Lett.* **1996,** *77*, 3865-3868.

5. Frisch, M. J.; Trucks, G. W.; Schlegel, H. B.; Scuseria, G. E.; Robb, M. A.; Cheeseman, J. R.; Scalmani, G.; Barone, V.; Petersson, G. A.; Nakatsuji, H.; Li, X.; Caricato, M.; Marenich, A. V.; Bloino, J.; Janesko, B. G.; Gomperts, R.; Mennucci, B.; Hratchian, H. P.; Ortiz, J. V.; Izmaylov, A. F.; Sonnenberg, J. L.; Williams; Ding, F.; Lipparini, F.; Egidi, F.; Goings, J.; Peng, B.; Petrone, A.; Henderson, T.; Ranasinghe, D.; Zakrzewski, V. G.; Gao, J.; Rega, N.; Zheng, G.; Liang, W.; Hada, M.; Ehara, M.; Toyota, K.; Fukuda, R.; Hasegawa, J.; Ishida, M.; Nakajima, T.; Honda, Y.; Kitao, O.; Nakai, H.; Vreven, T.; Throssell, K.; Montgomery Jr., J. A.; Peralta, J. E.; Ogliaro, F.; Bearpark, M. J.; Heyd, J. J.; Brothers, E. N.; Kudin, K. N.; Staroverov, V. N.; Keith, T. A.; Kobayashi, R.; Normand, J.; Raghavachari, K.; Rendell, A. P.; Burant, J. C.; Iyengar, S. S.; Tomasi, J.; Cossi, M.; Millam, J. M.; Klene, M.; Adamo, C.; Cammi, R.; Ochterski, J. W.; Martin, R. L.; Morokuma, K.; Farkas, O.; Foresman, J. B.; Fox, D. J. *Gaussian 16 Rev. C.01*, Wallingford, CT, 2016.

6. Te Velde, G.; Bickelhaupt, F. M.; Baerends, E. J.; Fonseca Guerra, C.; van Gisbergen, S. J.; Snijders, J. G.; Ziegler, T., Chemistry with ADF. *J. Comput. Chem.* **2001,** *22*, 931-967.

7. Kresse, G.; Joubert, D., From ultrasoft pseudopotentials to the projector augmented-wave method. *Phys. Rev. B* **1999,** *59*, 1758.

8. Ehrlich, S.; Moellmann, J.; Reckien, W.; Bredow, T.; Grimme, S., System-Dependent Dispersion Coefficients for the DFT-D3 Treatment of Adsorption Processes on Ionic Surfaces. *Comput. Phys. Commun.* **2011,** *12*, 3414-3420.

9. Heyd, J.; Scuseria, G. E.; Ernzerhof, M., Hybrid functionals based on a screened Coulomb potential. *J. Chem. Phys.* **2003,** *118*, 8207-8215.

10. Togo, A.; Tanaka, I., First principles phonon calculations in materials science. *Scr. Mater.* **2015,** *108*, 1-5.

11. van Lenthe, E.; Baerends, E.-J.; Snijders, J. G., Relativistic regular two-component Hamiltonians. *J. Chem. Phys.* **1993,** *99*, 4597-4610.

12. van Lenthe, E.; Baerends, E.-J., Optimized Slater-type Basis Sets for the Elements 1–118. *J. Comput. Chem.* **2003,** *24*, 1142-1156.

13. Adamo, C.; Barone, V., Toward reliable density functional methods without adjustable parameters: The PBE0 model. *J. Chem. Phys.* **1999,** *110*, 6158-6170.

14. Michalak, A. M., Mariusz; Ziegler, T., Bond Orbitals from Chemical Valence Theory. *J. Phys. Chem. A* **2008,** *112*, 1933-1939.

15. Grimme, S.; Antony, J.; Ehrlich, S.; Krieg, H., A consistent and accurate ab initio parametrization of density functional dispersion correction (DFT-D) for the 94 elements H-Pu. *J. Chem. Phys.* **2010,** *132*, 154104.

16. Mitoraj, M. P.; Michalak, A.; Ziegler, T., A Combined Charge and Energy Decomposition Scheme for Bond Analysis. *J. Chem. Theory Comput.* **2009,** *5*, 962-975.

17. Zhang, J.-X.; Sheong, F. K.; Lin, Z., Unravelling Chemical Interactions with Principal Interacting Orbital Analysis. *Chem. Eur. J.* **2018,** *24*, 9639-9650.

18. Zhang, J.-X.; Sheong, F. K.; Lin, Z., Principal interacting orbital: A chemically intuitive method for deciphering bonding interaction. *Wiley Interdiscip. Rev. Comput. Mol. Sci.* **2020,** *10*, e1469.

19. Sheong, F. K.; Zhang, J.-X.; Lin, Z., Principal interacting spin orbital: understanding the fragment interactions in open-shell systems. *Phys. Chem. Chem. Phys.* **2020,** *22*, 10076-10086.

20. Küchle, W.; Dolg, M.; Stoll, H.; Preuss, H., Energy-adjusted pseudopotentials for the actinides. Parameter sets and test calculations for thorium and thorium monoxide. *J. Chem. Phys.* **1994,** *100*, 7535-7542.

21. Cao, X.; Dolg, M.; Stoll, H., Valence basis sets for relativistic energy-consistent small-core actinide pseudopotentials. *J. Chem. Phys.* **2003,** *118*, 487-496.

22. VandeVondele, J.; Krack, M.; Mohamed, F.; Parrinello, M.; Chassaing, T.; Hutter, J., Quickstep: Fast and accurate density functional calculations using a mixed Gaussian and plane waves approach. *Comput. Phys. Commun.* **2005,** *167*, 103-128.

23. VandeVondele, J.; Hutter, J., Gaussian basis sets for accurate calculations on molecular systems in gas and condensed phases. *J. Chem. Phys.* **2007,** *127*, 114105.

24. Gernald, L.; Hutter, J.; Parrinello, M., A hybrid Gaussian and plane wave density functional scheme. *Mol. Phys.* **1997,** *92*, 477-488.

25. Lu, J.-B.; Cantu, D. C.; Xu, C.-Q.; Nguyen, M.-T.; Hu, H.-S.; Glezakou, V.-A.; Rousseau, R.; Li, J., Norm-Conserving Pseudopotentials and Basis Sets to Explore Actinide Chemistry in Complex Environments. *J. Chem. Theory Comput.* **2021,** *17*, 3360-3371.

26. Nosé, S., A unified formulation of the constant temperature molecular dynamics methods. *J. Chem. Phys.* **1984,** *81*, 511-519.

27. Hoover, W. G., Canonical dynamics: Equilibrium phase-space distributions. *Phys Rev A (Coll Park)* **1985,** *31*, 1695.

28. Sigmon, G. E.; Unruh, D. K.; Ling, J.; Weaver, B.; Ward, M.; Pressprich, L.; Simonetti, A.; Burns, P. C., Symmetry versus Minimal Pentagonal Adjacencies in Uranium-Based Polyoxometalate Fullerene Topologies. *Angew. Chem. Int. Ed.* **2009,** *48*, 2737-2740.